A new algorithm for unsupervised global and local color correction

Alessandro Rizzi [a,*], Carlo Gatta [a], Daniele Marini [b]

[a] *Department of Information Technology, University of Milano, Via Bramante 65, Crema (CR) 26013, Italy*
[b] *Department of Information Science, University of Milano, Via Comelico 39, Milano (Mi) 20100, Italy*

Abstract

In this work we present a new algorithm for digital images unsupervised enhancement with simultaneous global and local effects, called ACE for Automatic Color Equalization. It is based on a computational model of the human visual system that merges the two basic "Gray World" and "White Patch" global equalization mechanisms. Inspired by some adaptation mechanisms of the human vision, it realizes a local filtering effect by taking into account the color spatial distribution in the image. Like the human visual system, ACE is able to "adapt" to widely varying lighting conditions and to extract visual information from the environment efficaciously. It has shown promising results in achieving different equalization tasks, e.g. performing color and lightness constancy, realizing image dynamic data driven stretching, controlling the contrast. Characteristics, tests and results are presented.
© 2002 Elsevier Science B.V. All rights reserved.

Keywords: Image enhancement; Color equalization; Color constancy

1. Introduction

One of the abilities of the human visual system is to steadily perceive a scene regardless of the changes in lighting conditions; we refer to this phenomenon as *color constancy* (Wyszecky and Stiles, 1982). However, while the human visual system stabilizes perception when there are illuminant variations, from another view point human visual system makes the perception of object's reflectances dependent on the chromatic and spatial composition of the scene (Albers, 1975; DeValois and DeValois, 1988). Thus the final visual appearance can not be explained with just a global approach; identical visual stimuli in different contexts can originate different visual appearances.

The goal of these mechanisms is to maximize the image's dynamics, as well as the information content of the perceived scene. Following this consideration, the basic idea of this work is to develop a digital image automatic enhancement algorithm that mimics some characteristics of the human visual system, in particular, color constancy and lightness constancy, not considering all its complex inner mechanisms. However, some adaptation properties can be described by low level principles like chromatic channels independent

---

* Corresponding author.
E-mail addresses: rizzi@dti.unimi.it (A. Rizzi), gatta@ dti.unimi.it (C. Gatta), daniele.marini@unimi.it (D. Marini).

adaptation (McCann, 1999), White Patch (von Kries, 1970) and Gray World (Buchsbaum, 1980) adapting behavior, lateral inhibition mechanism (Hartline et al., 1956) and local–global adaptation (McCann, 1987).

In some cases the human visual system normalizes its channel values, maximizing toward a hypothetical white reference area, achieving color constancy. We refer to this mechanism as *White Patch*. When the mean luminance of the scene changes, our visual system performs various mechanisms to adapt to the new condition. This allow us to have comparable luminance perception despite this change. In photography this is done by modifying lens aperture and shutter time, in order to acquire the image with gray levels fitted on the available dynamic. In the imaging field, when this happens independently between the three chromatic channels, some global chromatic dominant can be eliminated. We refer to this mechanism as *Gray World*. This correction mechanism is an important component of the adaptation process, but if used as stand alone model, it fails to achieve color constancy in some cases (Rizzi et al., 2002), among them when Gray World assumption is not respected. We recall the difference between Gray World and White Patch mechanisms and Gray World and White Patch assumptions. The first ones are properties of image correction algorithms while the latter are properties of images to be corrected. These assumptions are respected for White Patch when a white area is present in the scene and for Gray World when all the tones in the scene can be represented in an image with a gray mean value, keeping the visual naturalness of the scene. At first sight, White Patch and Gray World can be considered as competing processes, but they can actually be part of the same model.

Channel independence, Gray World and White Patch mechanisms do not account for all the aspects of visual appearance: we need to also take into account spatial relationships in the scene, like other models do (McCann, 1999; Land and McCann, 1971; Spitzer and Sherman, 2002). In fact, visual appearance not only depends on the above mentioned adaptation mechanisms. Other complex mechanisms are involved in producing the final visual result; among them perceptual spatial interaction like assimilation and contrast (Adelson, 1993).

ACE aims to model a simplified version of the inner complex behavior of the human visual system, reproducing in a qualitative way the above mentioned adaptation mechanisms. It has been devised primarily for the enhancement of digital images, characterized by a lower dynamic range compared to the high range of real world scenes. For this reason, a quantitative assessment of the model has not been carried out so far, it is matter for further research.

To differentiate the real process from its model, we use the word *adaptation* to indicate the biological adaptations made by the human visual system in the real world and the word *adjustment* to indicate the simplified adaptations of ACE in the digital images domain. In this paper the term *adjustment* will always refer to this meaning.

2. Computing the visual appearance

In order to approximate the visual appearance of a scene, we have considered in our model mechanisms of spatial interaction like lateral inhibition and local–global contrast. We developed a model trying to simultaneously combine in a unique computation some of the mechanisms involved in the human visual perception (Gatta et al., 2002). Within this model, every basic principle is considered as part of a unique adaptive behavior involving the contribution of each mechanism to the final result. Each adaptive mechanism has global and local effects as a consequence of a number of simple local operations across the image.

The algorithm has been implemented following the scheme shown in Fig. 1. The first stage accounts for chromatic spatial adjustment, which is responsible for color constancy and contrast tuning while a second stage configures the output range to implement an accurate tone mapping, performing lightness constancy. The first stage merges the Gray World and White Patch approaches performing a kind of lateral inhibition mechanism, weighted by pixel distance. The result is a local–global filtering. The second stage maxi-
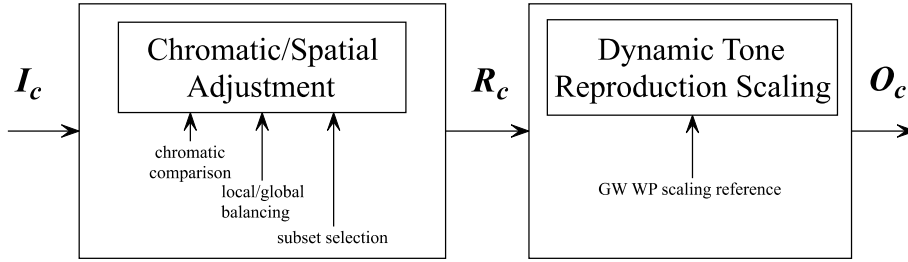
Fig. 1. Basic algorithm structure.

mizes the image dynamic, normalizing the white at a global level only. This two-phase structure is a characteristic in a majority of the human visual system computational models in the field of digital imaging (Hurlbert, 1986; Pattanaik et al., 1998). This algorithm requires no user supervision, no statistic characterization and no data preparation.

In Fig. 1, I is the input image, R is an intermediate result and O is the output image while subscript c denotes the chromatic channels.

2.1. Chromatic/spatial adjustment

In the first stage, the chromatic/spatial adjustment produces an output image R in which every pixel is recomputed according to the image content. Each pixel p of the output image R is computed separately for each channel c as follows:

$$R_c(p) = \sum_{j \in \text{Subset}, j \neq p} \frac{r(I_c(p) - I_c(j))}{d(p, j)} \quad (1)$$

where $I_c(p) - I_c(j)$ accounts for the lateral inhibition mechanism, $d(\cdot)$ is a distance function which weights the amount of local or global contribution, $r(\cdot)$ is the function discussed below that accounts for the relative lightness appearance of the pixel.

The pixel computation can be extended to the whole image or restricted to a Subset. In all the examples and data presented in the paper the whole image has been used. Tests are in progress to select random or pre-computed image subsets in order to accelerate the computation.

In the basic formula 1 no compensation is computed for the distance of the pixel from the edge. Consequently, Eq. (1) has been modified with a normalization coefficient in the following way:

$$R_c(p) = \frac{\sum_{j \in \text{Subset}, j \neq p} \frac{r(I_c(p) - I_c(j))}{d(p, j)}}{\sum_{j \in \text{Subset}, j \neq p} \frac{r_{\max}}{d(p, j)}} \quad (2)$$

where $r_{\max}$ is the maximum value of $r(\cdot)$.

The lateral inhibition mechanism is simulated by computing the difference between each pixel value and all other pixels of the selected image subset. This difference is tuned by the function $r(\cdot)$, later presented.

2.1.1. Global/local weight: the $d(\cdot)$ function

The distance $d(\cdot)$ weights the global and local filtering effect, both present in the human visual system. Global models, in fact, are not able to simulate several local chromatic adaptation effects, e.g. the simultaneous contrast or the Cornsweet effect (Cornsweet, 1970).

Initial tests of the algorithm have been performed using the Euclidean distance (Ed), but alternative functions have been tested. A preliminary comparison is shown in Fig. 2. Some of the tested distances include *Euclidean*, *inverse exponential*, *Manhattan*, *maximum*, *Euclidean*, *Manhattan*[2], *maximum*[2], *Euclidean*[3]. Tested distances are shown in Table 1, where dx and dy are the horizontal and vertical distances between two pixels.

While only the last two distances in Fig. 2 gave unsatisfactory results, some functions seem to achieve better results than others even though there was no absolute definitive function found. For the tests in this paper we have chosen the Euclidean distance Ed, so the distance weighting function $1/\text{Ed}$ has the shape shown in Fig. 3. The choice of the distance function requires more investigation; tests are in progress to compare Ed and inverse exponential.

Fig. 2. Sample image filtered with different $d(\cdot)$ function.

Table 1
Tested distances

Euclidean	Inverse exponential	Manhattan	Maximum
$\sqrt{(\mathrm{d}x^2 + \mathrm{d}y^2)}$	$\dfrac{1}{e^{-\alpha Ed}}$	$\mathrm{d}x + \mathrm{d}y$	$\mathrm{Max}(\mathrm{d}x, \mathrm{d}y)$

2.1.2. Tuning the contrast: the relative lightness appearance function r(·)

For each pixel in the image, $r(\cdot)$, together with $d(\cdot)$, controls the relative pixels influence, ac-

counting for the spatial channel lightness adjustment. They compute all the single contributions of the image content to each final pixel value in the output image. To perform a Gray World behavior,
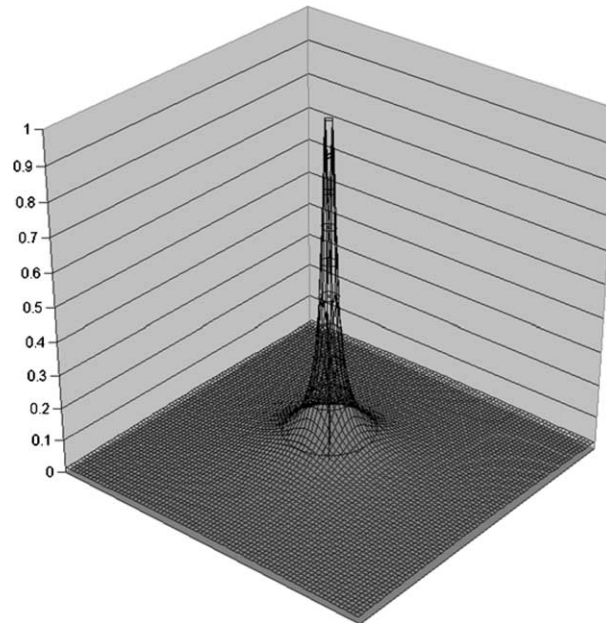
Fig. 3. 3D shape of the weighting function 1/Ed.

$r(\cdot)$ has to be an odd function, while the White Patch behavior is obtained by non-linear enhancements of relative differences between pixels. The non-linearity of $r(\cdot)$ derives from its saturation. This mechanisms does not affect the final channel saturation, since this formula computes the influence of only one pixel and has to be calculated for all the pixel in the image (or chosen subset). The channel saturation only depends on the final stage of dynamic tone reproduction scaling, further described.

We have tested different $r(\cdot)$ functions, trying to implement an effective White Patch mechanism. Fig. 4 displays the tested functions. Linear and Signum functions can be seen as limit cases of a Saturation function with unitary or infinite slope respectively.

The variation of the slope of the function $r(\cdot)$ acts as a contrast tuner. It can be seen in the $r(\cdot)$ function comparison shown in Fig. 5. The higher the slope is, the higher the contrast.

To test the $r(\cdot)$ functions color correction capabilities, the mean ΔE distance in CIELab (Wyszecky and Stiles, 1982) between two synthetic images of a living room, computed with a photometric ray tracer (Marini et al., 1999) under the A and D65 CIE illuminant, before and after the filtering has been computed. The results are shown in Table 2,
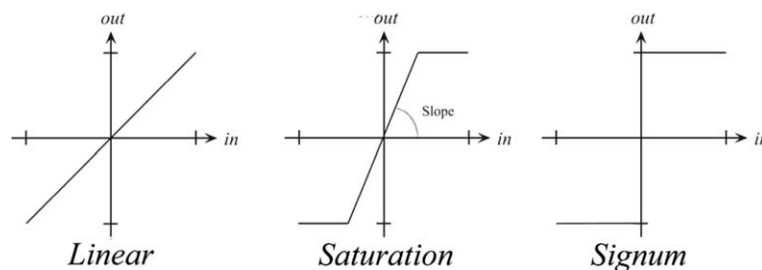
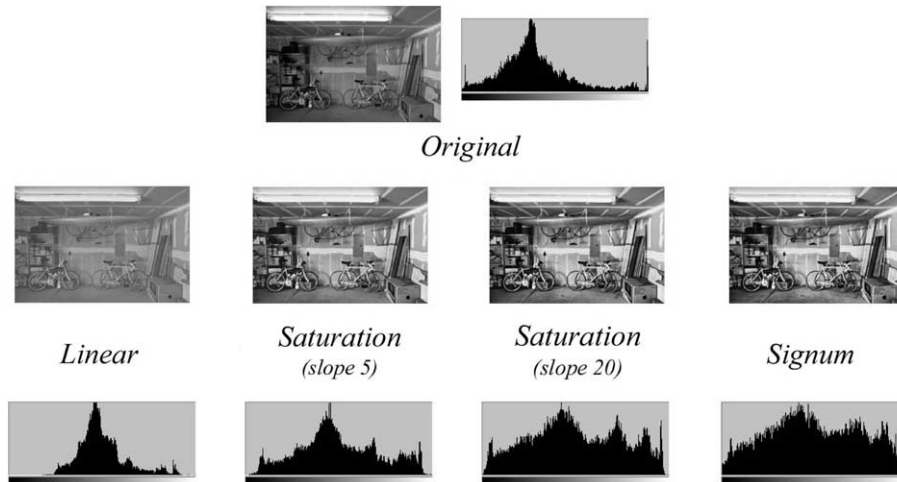Fig. 4. Tested $r(\cdot)$ functions.

Fig. 5. Sample image filtered with different $r(\cdot)$ function.

Table 2
Mean ΔE distance between two synthetic images under the A and D65 CIE illuminant, without any filtering (Original) and filtered with the various $r(\cdot)$ functions

Original	Linear	Signum	Saturation
48.74	7.26	4.54	6.94

The Signum function performs the most effective color correction, but it increases the contrast considerably, as shown in the enlarged detail of Fig. 6. "S" shaped $r(\cdot)$ functions with the same slope mechanisms are under tests.

2.2. Dynamic tone reproduction scaling

The second stage maps the intermediate pixels matrix R into the final output image O. In this stage, not only can a simple dynamic maximiza-tion be made (linear scaling), but also different reference values can be chosen in the intermediate matrix to map into gray levels the relative lightness appearance values of each channel. According to the chosen reference point, an additional global balance between Gray World and White Patch can be added. Two linear scaling methods are pro-posed to obtain a standard 24 bit output image from the signed floating point matrix R. However, alternative scaling methods can be used to take into account non-linearities typical of the human lightness adaptation, without changing ACE two-phases structure.

2.2.1. Linear scaling

This simple method linearly scales the range of values in R_c independently in the relative channel c into the range $[0, 255]$ using the formula:
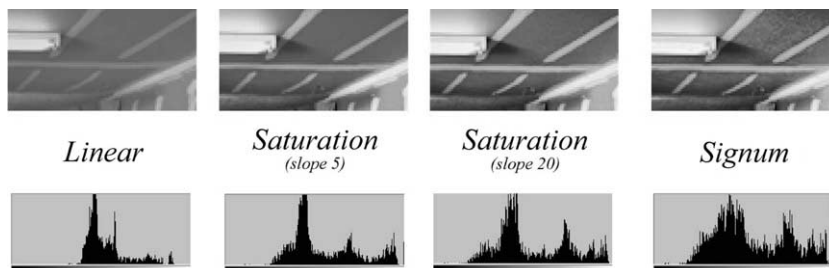
Fig. 6. Enlarged details of a synthetic image filtered using various $r(\cdot)$ functions.

$$O_c(p) = \text{round}[s_c(R_c(p) - m_c)] \qquad (3)$$

for each pixel p where s_c is the slope of the segment $[(m_c, 0), (M_c, 255)]$, with $M_c = \max_p R_c(p)$ and $m_c = \min_p R_c(p)$.

In this case the linear mapping fills the available dynamic range without further adjustment.

2.2.2. White Patch/Gray World scaling

This alternative method yields better results linearly scaling the values in R_c with the formula 4 using M_c as white reference and the zero value in R_c as an estimate for the medium gray reference point to compute the slope s_c. For this reason, the available dynamic could not be used in its entirety and tones around the very dark values could be lost. Alternatively, some values in O_c can result negative. In this case the values lower than zero are set to zero.

$$O_c(p) = \text{round}[127.5 + s_c R_c(p)] \qquad (4)$$

This second method adds a global Gray World adjustment in the final scaling, thus the dynamic of the final image is always centered around the medium gray.

3. ACE filtering characteristics

In this section we present an overview of the more significant ACE characteristics. In fact, its automatic and unsupervised color correction are the result of different properties. Some of these properties depend on the algorithm's parameters,

others depend on the image content. Quantitative measures of some of these properties are presented. Unless differently specified, all the results presented in this paper have been filtered using the following parameters: whole image as subset in formula 2, Saturation function with slope 20 as $r(\cdot)$, Euclidean distance as $d(\cdot)$, WP/GW scaling in the second stage.

3.1. Lightness constancy and dynamic modification

Most of the color correction algorithms that "search for the white" increase the overall lightness of the image in every case. On the contrary, ACE, due to its Gray World behavior component, is able to modify the lightness according to its original value. In Fig. 7 two examples of ACE filtering are shown. In the first image, that is slightly under-exposed, ACE increases the mean lightness, while in the second one, that is over-exposed, ACE reduces the lightness.

The effect of the algorithm on the image dynamic can be seen in Fig. 8, where the same image with its histogram is shown before and after the ACE filtering.

Quantitatively, ACE effects on lightness and dynamic can be seen in Table 3, where *histogram flatness* is the L1 distance between the image histogram and a flat histogram on the same image dimension, *percentage used dynamic* is the percentage of the used values in the available dynamic range, *percentage unused black* and *percentage unused white* are the percentage of contiguous
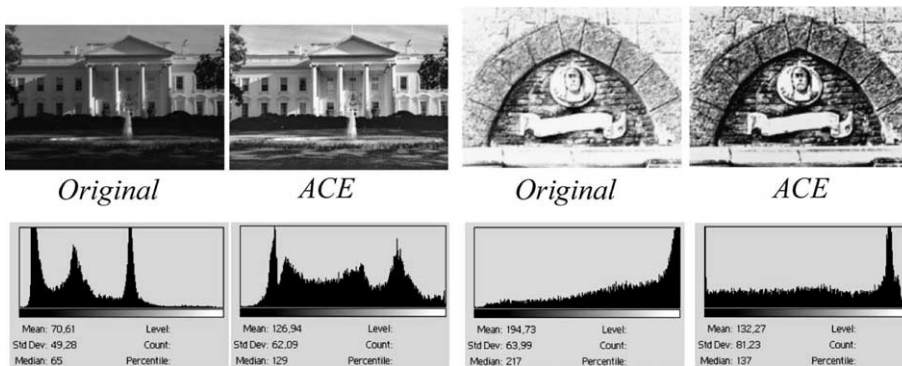

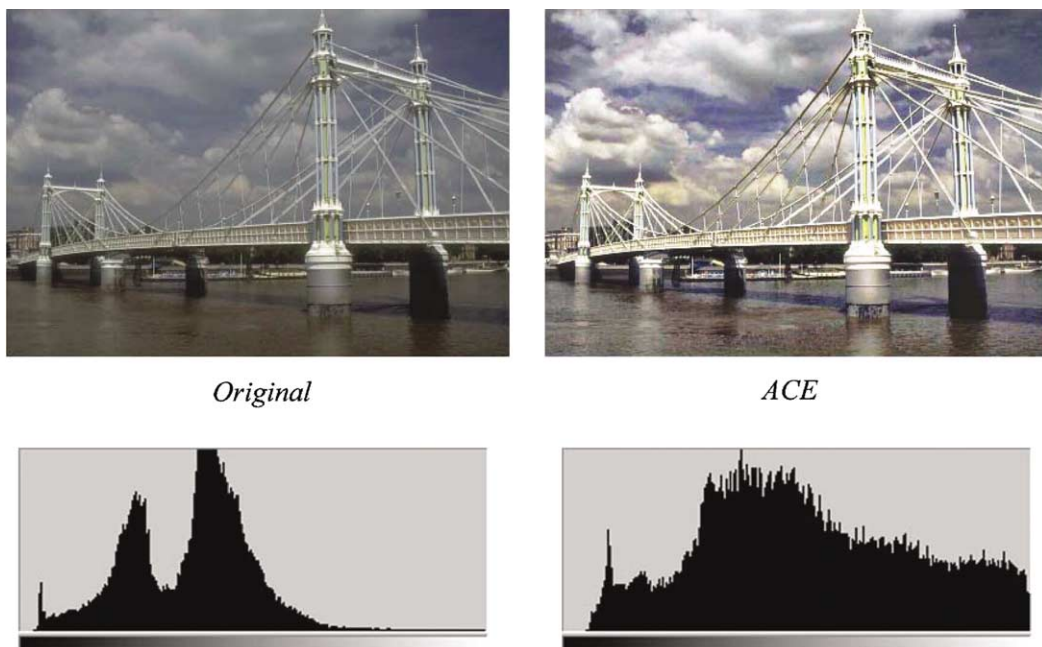Fig. 7. ACE lightness constancy effect.

Fig. 8. Dynamic range of an image before and after ACE filtering.

Fig. 9. Visual comparison of ACE filtering on the synthetic images.

Table 3
Lightness and dynamic data of the two images in Fig. 7 in the same order

	Orig	ACE	Orig	ACE
Mean	70.61	126.94	194.73	132.27
Histogram flatness	38249.38	17151.75	48669.59	22442.88
Percentage used dynamic	93.36	97.26	98.83	99.61
Percentage unused black	0.39	0	1.17	0
Percentage unused white	3.90	0	0	0

unused values in the lower and upper part of the histogram respectively. Histogram flatness values are not normalized to the image dimension since we are interested in comparing differences of this value on the same image, before and after the ACE filtering: lower values correspond to flatter histograms.

As it can be noticed from values in Table 3, ACE moves lightness mean towards medium gray and increase the percentage of used dynamic and the flatness of the histogram.

3.2. Color constancy

In order to measure the algorithm's ability to perform *color constancy*, we have computed the mean ΔE (Wyszecky and Stiles, 1982) distance across all the corresponding pixels between two images of the same size:

$$\Delta E_{\text{mean}} = \frac{\sum_{p \in \text{Image}} \Delta E(I_1(p), I_2(p))}{sizex \cdot sizey}$$

where I_1 and I_2 are the images to be compared, *sizex* and *sizey* are the image dimension in pixels.

From the mathematical point of view, this measure allows idealized color constancy. $\Delta E = 0$ indicates a perfect discount of the illuminant and consequently an absolute perception of the objects reflectance. Such a separation between illuminant spectral distribution and objects spectral reflectance does not happen in real conditions: human visual system performs significant, but incomplete adaptation (McCann et al., 1976). Thus, the significance of this measure comes from the variation of its value after the adjustment.

For the tests, we have used two image sets: the University of East Anglia (UEA) uncalibrated color image database and a set of six synthetic images generated by a photometric ray tracer program from the same 3D scene in six different lighting conditions. The UEA uncalibrated color image database is a database of 392 design images made from 28 different designs images under three light sources using four digital cameras and two commercial scanners arbitrarily chosen. The images were acquired under a CIE A, D65 and TL84 lights. In this paper we used only the image set acquired with the Fuji Mx-700 digital camera. The six synthetic images were generated with a photometric raytracing algorithm (Marini et al., 1999) from a 3D living room model. The light sources used were the standard Cie illuminant A, B, C, D65 and a Hg lamp; the latter image was obtained using a mix of these illuminants.

On the synthetic image set, we have measured the mean ΔE chromatic distance for any couple of illuminants before (Table 4) and after the ACE filtering (Table 5).

A visual comparison of the ACE filtering on the synthetic images is shown in Fig. 9. As it can be noticed, the chromatic dominant of the illuminant is strongly reduced. In the image with more than one illuminant ACE leaves some local color bleeds. This result is in line with the human behavior in which the chromatic adaptation fails, and we can notice easily the illuminant color, if different illuminants are present in the field of view.

The same measures have been done on the UEA uncalibrated color image database, on every pattern, obtaining the results summarized in Table 6.

Since ACE realizes low level HVS mechanisms, it is not able to distinguish an orange cast due to a tungsten illuminant from the orange of a sunset landscape. In the case of images with a natural strong dominant color (i.e. underwater images, sunsets, etc.), filtering with ACE eliminates the natural color dominant producing a chromatic

Table 4
Mean ΔE on the original synthetic images

Before	A	B	C	D65	Hg	Mix
A	0					
B	36.12	0				
C	52.56	17.06	0			
D65	48.56	12.51	6.45	0		
Hg	46.1	18.42	21.05	19.15	0	
Mix	27.1	9.52	25.76	21.55	24.49	0

Table 5
Mean ΔE on the ACE filtered synthetic images

Filtered	A	B	C	D65	Hg	Mix
A	0					
B	6.19	0				
C	7.22	1.81	0			
D65	6.94	1.68	1.33	0		
Hg	8.48	5.05	5	5.09	0	
Mix	8.74	8.08	8.63	8.46	10.34	0

distorted image. Similar problem can occur with particular images far from both the gray world and the white patch assumptions. To solve this problem, a higher level scenes classification program can be used before the ACE filtering to detect these cases and avoid the filtering or filter with a conservative parameter tuning to preserve the original image color.

3.3. Global and local filtering effect

ACE performs simultaneously global and local filtering. In the example of Fig. 10, ACE eliminates the global green dominant, due to the illumination of the scene. This color correction could not be obtained using a global algorithms like White Patch. In fact, in the right upper corner of the image there is visible a white spot. Applying the White Patch global algorithm in presence of a white pixel produces an unchanged image.

In Fig. 11 the local effect of ACE is shown. The pixel differences (bottom Fig. 11) between the original and the ACE filtered images (top Fig. 11) are visualized around the 128 gray and are shown separately for each chromatic channel. Pixels with different gray values have been changed differently; this indicates the ACE local filtering effect.

The ACE local effect is visible also in Fig. 12, where histograms of RMS error (in RGB) and ΔE (in CIELab) computed for each couple of corresponding pixels between the original and the ACE output of Fig. 11 are drawn. The width of these curves is an index of the numerical and perceptual locality of ACE filtering.

3.4. Contrast modification

Several definitions of image contrast have been proposed so far, but the concept of perceived contrast is still a matter of discussion in the field of digital imaging as well as in the psycho-physics. Classic definitions (e.g. Weber, Michelson), used in several research fields (Michelson, 1927; Jain, 1989; Peli, 1997), are limited to a global notion of contrast that does not take into account essential local properties of perceived contrast in images.

In ACE the parameter which is responsible of the contrast modification is the relative lightness appearance function $r(\cdot)$ which is a local operator. This results in a contrast modification which can have independent global and local effects. In Fig. 13 an ACE filtering example is shown; the global contrast decreases while the local one increases, as visible in the image details.

Table 6
Mean ΔE on the UEA images, across the illuminants, before and after the ACE fltering, with the relative decreasing ratio

N	Before	After	After/before
1	40.72	19.73	0.48
2	44.34	17.23	0.39
3	40.39	26.69	0.66
4	41.76	15.53	0.37
5	–	–	–
6	37.64	18.66	0.5
7	42.11	20.53	0.49
8	41.30	15.20	0.37
9	45.15	25.33	0.56
10	41.96	26	0.62
11	39.53	17.29	0.44
12	47.97	23.05	0.48
13	48.26	24.6	0.51
14	39.84	14.06	0.35
15	38.54	11.52	0.3
16	39.96	13.61	0.34
17	47.12	28.37	0.6
18	42.7	30.97	0.73
19	41.49	15.34	0.37
20	47.89	25.26	0.53
21	43.19	22.03	0.51
22	38.18	17.47	0.46
23	41.16	22.46	0.55
24	40.27	20.11	0.5
25	43.18	18.27	0.42
26	39.87	15.95	0.4
27	44.78	37.29	0.83
28	42.12	27.66	0.66
Mean	42.27	21.12	0.5

3.5. Data driven color dequantization

Using ACE to filter an image with a limited color palette, results in a data driven color dequantization. This interesting property derives from its local behavior, according to which all the pixels are recomputed in relation to the rest of the image with a weighting mechanisms that gives more importance to near pixels. This local recomputation is the criterion for the final spatial distribution in the image of the histogram original quantized value. In the example shown in Fig. 14 liner scaling has been used.

3.6. Following the human vision

We have tested the algorithm on some classic visual illusions in order to verify whether the ACE model behaves qualitatively like the human visual system. Alternative computational models have been tested in a similar way (Marini and Rizzi, 2000).

Two visual configurations have been chosen that originate simultaneous contrast and Cornsweet effect respectively. These configurations and the relative ACE outputs are shown in Figs. 15 and 16. Notice that both the ACE computations follow qualitatively the expected visual appearance of the two configurations. Quantitative measures of these shifts will be matter of further research.
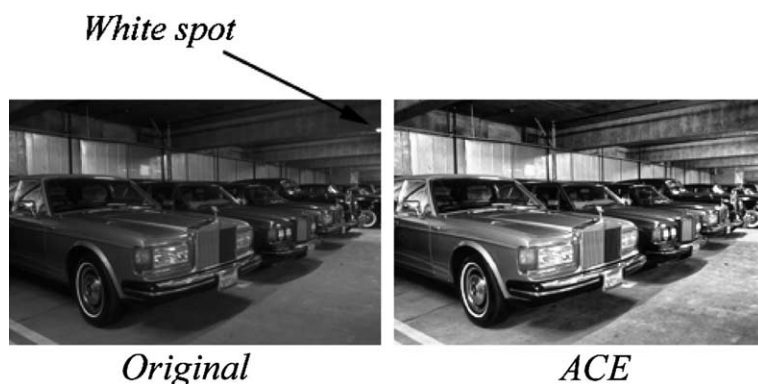

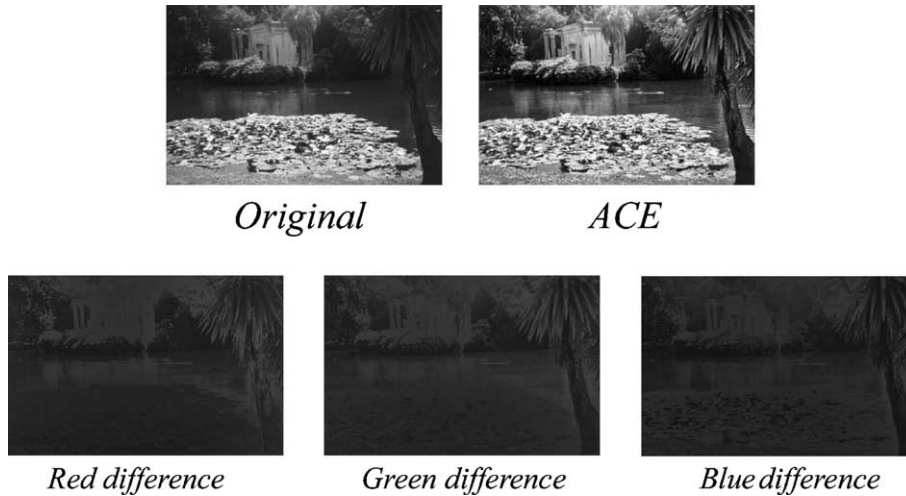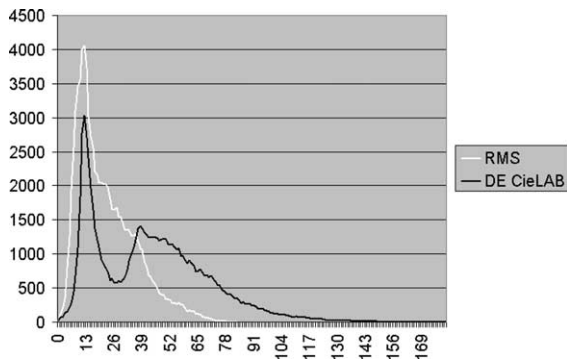Fig. 10. ACE color constancy effect in presence of white pixels.

Fig. 11. ACE local filtering effect.

Fig. 12. RMS (in RGB) and ΔE (in CIELab) histograms between the original and the ACE output of Fig. 11.

3.7. ACE computational time

The basic ACE algorithm, which has not been optimized, has an $O(N^2)$ computational cost where N is the pixels number of the image. On a PIII@700Mhz, running Windows 2000, takes 8.5″ to compute a 100×75 pixels image and 6′44″ to compute a 192×192 pixels image. These data refer to computations in which the whole image is used as subset in formula 2.

A multilevel approach or an automatic selection of image subsets are two of the possible driving lines for its optimization. Tests are in progress to select random or pre-computed image subsets in order to accelerate the computation.

Regarding the first approach, an optimized version of the algorithm based upon a local linear look up table (LLL) speed-up technique (Rizzi and Gatta, 2002) has been developed and is currently under test. The idea underlying the LLL method, shown in Fig. 17, is to apply the ACE algorithm to a small sub-sampled version of the original image and to create three LUT mapping functions (for R, G and B) between the two sub-sampled images (the ACE filtered and the original sub-sampled one). These mapping functions are then used to quickly filter the original full size image, generating each pixel in the final color corrected image, via a local interpolation on the LUT values, separately on each chromatic channel.

At a preliminary analysis, this speed-up method has given promising results. A visual comparison of the basic and LLL–ACE algorithms do not reveal significant differences (see Fig. 18) while the computational times are strongly reduced (2″ for the image 192×192 and almost instantaneous for the image 100×75, using a scaling factor 4).

4. Conclusions and perspectives

A new algorithm for unsupervised digital image color equalization, called ACE, has been presented. It derives from a new model that tries to mimic relevant adaptation behaviors of the human
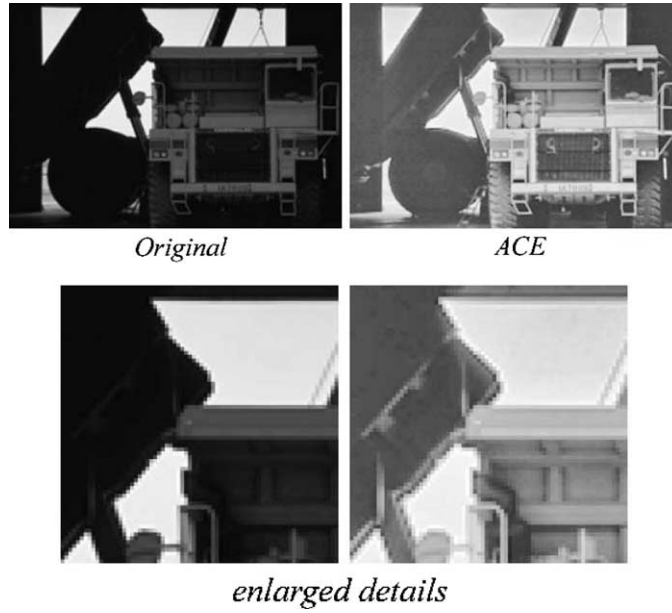
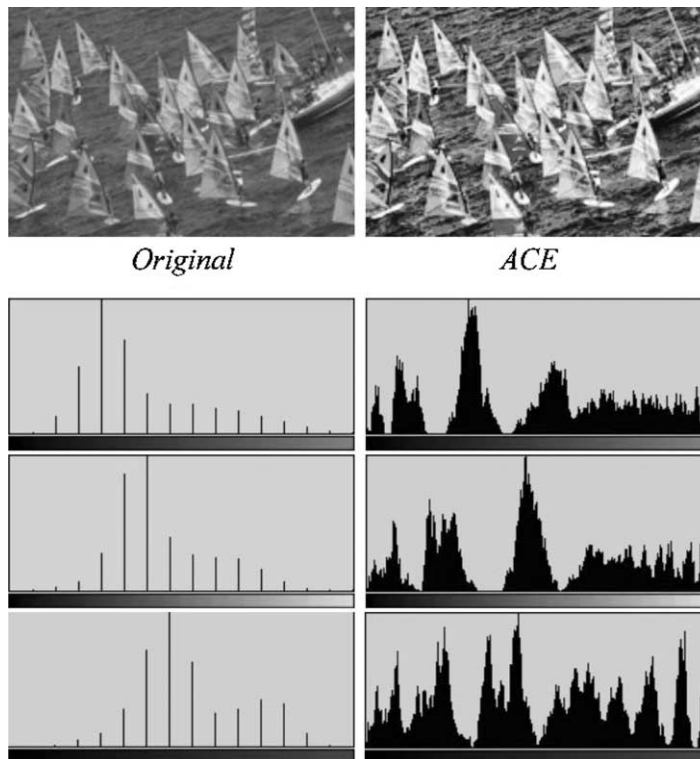Fig. 13. ACE global and local contrast modification effect.

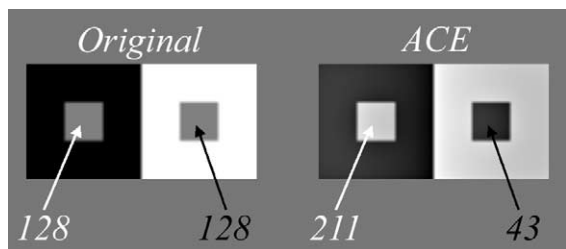Fig. 14. ACE color dequantization (linear scaling).

Fig. 15. Simultaneous contrast visual configuration and the relative ACE filtering.

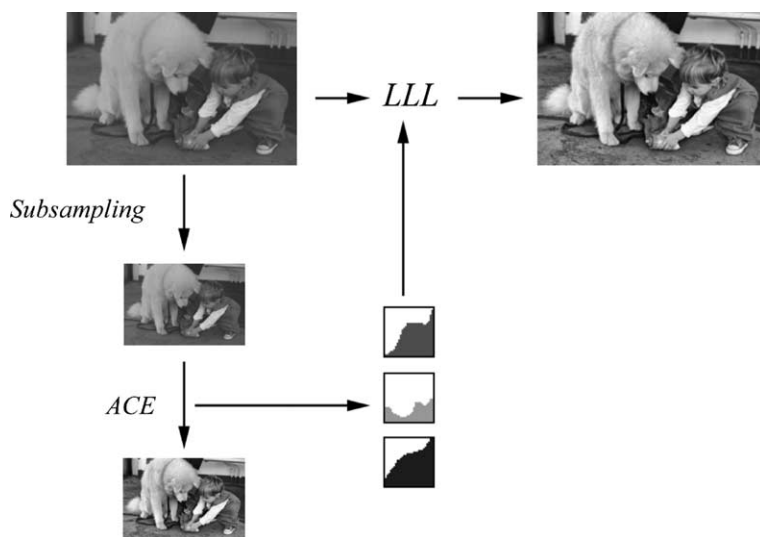Fig. 16. Cornsweet effect and the relative ACE filtering.
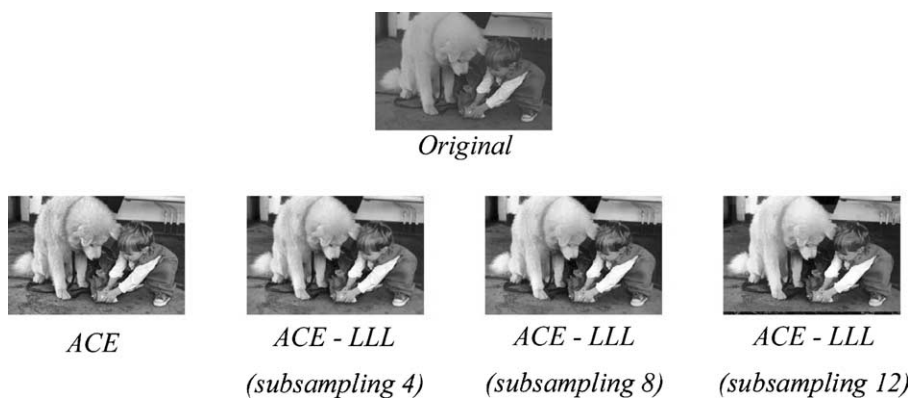

Fig. 17. Local linear LUT ACE scheme.

Fig. 18. Local linear LUT ACE and basic ACE visual comparison.

visual system, such as lightness constancy and color constancy. The first phase of visual encoding, recovers the appearance of the scene areas and the second phase of display mapping normalizes the values of the filtered image, maximizing its dynamic.

Results are promising: ACE has proven to achieve an effective color constancy correction and a satisfactory tone equalization performing simultaneously global and local image correction. However, ACE is an ongoing research; to tune some of its internal functions and parameters further investigation is required. In particular, different weighting distances $d(\cdot)$, relative lightness appearance functions $r(\cdot)$ and alternative linear and logarithmic tone reproduction scaling methods are under test. The computational cost of the basic algorithm is very high. To overcome this limitation a multilevel version has been developed; also its performance is under test.

References

Adelson, E., 1993. Perceptual organization and the judgment of brightness. Science, 2042–2044.

Albers, J., 1975. Interaction of Color. Yale University Press, New Haven.

Buchsbaum, G., 1980. A spatial processor model for object color perception. J. Franklin inst. 310 (1), 1–26.

Cornsweet, T., 1970. Visual Perception. Academic Press, New York.

DeValois, R.L., DeValois, K., 1988. Spatial Vision. Oxford University Press, New York.

Gatta, C., Rizzi, A., Marini, D., 2002. Ace: An automatic color equalization algorithm. In: Proceedings of the CGIV02 the First European Conference on Color in Graphics Image and Vision Poitiers, France.

Hartline, H.K., Wagner, H.G., Ratcliff, F., 1956. Inhibition in the eye of limulus. J. General Physiol. 39 (5), 651–673.

Hurlbert, A.C., 1986. Formal connections between lightness algorithms. J. Opt. Soc. A 3, 1684–1693.

Jain, A.K., 1989. Fundamentals of digital image processing. Prentice Hall, Englewood Cliffs.

Land, E., McCann, J., 1971. Lightness and retinex theory. J. Opt. Soc. Am. 61, 1–11.

Marini, D., Rizzi, A., Rossi, M., 1999. Color constancy measurement for synthetic image generation. J. Electron. Imaging 8 (4), 394–403.

Marini, D., Rizzi, A., 2000. A computational approach to color adaptation effects. Image Vis. Comput. 18, 1005–1014.

McCann, J.J., 1987. Local/global mechanisms for color constancy. Die Farbe 34, 275–283.

McCann, J.J., 1999. Lesson learned from mondrians applied to real images and color gamuts. In: Proceedings of the IS&T/SID 7th Color Imaging Conference.

McCann, J.J., McKee, S.P., Taylor, T.H., 1976. Quantitative studies in retinex theory—a comparison between theoretical predictions and observer responses to the color mondrian experiments. Vis. Res. 16, 445–458.

Michelson, A.A., 1927. Studies in optics. University of Chicago Press.

Pattanaik, S.N., Ferwerda, J.A., Fairchild, M.D., Greenberg, D.P., 1998. A multiscale model of adaptation and spatial vision for realistic image display. In: Proceedings of the SIGGRAPH98 Orlando, Florida, USA.

Peli, E., 1997. In search of a contrast metric: Matching the perceived contrast of gabor patches at different phases and bandwidths. Vis. Res. 37 (23), 3217–3224.

Rizzi, A., Gatta, C., Marini, D., 2002. Color correction between gray world and white patch. In: Proceedings of the Electronic Imaging 2002, S. Jose, California, USA.

Rizzi, A., Gatta, C., 2002. A local linear lut method for increasing the speed of generic image filtering algorithms. Technical report, University of Milano, Milano, Italy.

Spitzer, H., Sherman, E., 2002. Color contrast: A biological model and its application for real images. In: Proceedings of the CGIV02 the First European Conference on Color in Graphics Image and Vision Poitiers, France.

von Kries, J., 1970. Sources of color science. In: MacAdam, David L. (Ed.), Chromatic Adaptation. MIT Press, Cambridge, MA, pp. 109–119.

Wyszecky, G., Stiles, W.S., 1982. Color Science: Concepts and Methods, Quantitative Data and Formulas. J. Wiley & Sons, New York.